Research Article

Enhanced Supercapacitance of Hydrous Ruthenium Oxide/Mesocarbon Microbeads Composites toward Electrochemical Capacitors

Changzhou Yuan, Linrui Hou, Diankai Li, Long Yang, and Jiaoyang Li

Anhui Key Laboratory of Metal Materials & Processing, School of Materials Science & Engineering, Anhui University of Technology, Ma'anshan 243002, China

Correspondence should be addressed to Changzhou Yuan, ayuancz@163.com

A facile hydrothermal strategy was proposed to synthesize $RuO_2 \cdot nH_2O$/mesocarbon microbeads (MCMBs) composites. Further physical characterizations revealed that $RuO_2 \cdot nH_2O$ nanoparticles (NPs) were well dispersed upon the surfaces of the MCMB pretreated in 6 M KOH solution. Electrochemical data indicated that the $RuO_2 \cdot nH_2O$/MCMB composites owned higher electrochemical utilization of RuO_2 species, better power property, and better electrochemical stability, compared with the single RuO_2 phase. The good dispersion of $RuO_2 \cdot nH_2O$ NPs and enhanced electronic conductivity made the H^+ ions and electrons easily contact the $RuO_2 \cdot nH_2O$ phase for efficient energy storage at high rates.

1. Introduction

Electrochemical capacitors (ECs) are a kind of charge-storage devices possessing higher power density, more excellent reversibility, longer life cycle than batteries and much higher energy density compared to conventional capacitors [1]. Owing to these extraordinary properties, ECs have attracted increased interests during the past years with projected applications in the hybrid vehicle systems and memory backup systems. The electrochemical performance of ECs depends upon the electroactive materials greatly. Among these electroactive materials, hydrous ruthenium oxide ($RuO_2 \cdot nH_2O$) has been recognized as the state-of-the-art electrode material, due to its facile transport pathways for both protons and electrons, high specific capacitance (SC), highly reversible redox reactions, and so forth, [2–8]. However, a very high cost and toxic nature greatly preclude its commercial application. For this reason, the approaches to reduce its amount and further enhance its electrochemical utilization are essential to make the RuO_2-based devices more cost-effective.

It is well established that the good dispersion of $RuO_2 \cdot nH_2O$ nanoparticles (NPs) upon the surface of the carbon matrices is much favorable for enhancing their electrochemical utilization [4–8]. And the $RuO_2 \cdot nH_2O$/carbon-based composites delivered a wide SC range from 150 to 1580 F g^{-1} [5, 8], which was greatly depending upon the loading and thickness of the $RuO_2 \cdot nH_2O$ existing in the carbon materials. Commonly, the used carbon materials include carbon nanotubes [4], activated carbon [5], carbon black [6], and carbon nanofibres [7]. Since mesocarbon microbeads (MCMB) were first separated by Honda and Yamada from the mesophase pitches [9], this typical carbon material has been used in many applications, such as high-density carbon material [10, 11], filler for high-performance liquid chromatography [12], active carbon with super high surface [13], anodes of lithium ion battery [14–18], alkaline zinc-air cells [19], and supports of NiO NPs for ECs [20].

To the best of our knowledge, the investigation of the MCMB as a support to disperse $RuO_2 \cdot nH_2O$ NPs for ECs has not been reported as yet. In this work, the $RuO_2 \cdot nH_2O$ NPs were well dispersed upon the surfaces of the MCMB *via* mild hydrothermal method. Such unique $RuO_2 \cdot nH_2O$/MCMB composites can not only enhance the dispersion of $RuO_2 \cdot nH_2O$ NPs but remit their serious aggregation

meanwhile. Furthermore, the micrometer size of $RuO_2 \cdot nH_2O$/MCMB composites greatly favors for their practical fabrication. Electrochemical performance of the $RuO_2 \cdot nH_2O$/MCMB composites was systematically investigated in 0.5 M H_2SO_4 aqueous solution. Electrochemical data indicated that the $RuO_2 \cdot nH_2O$/MCMB composites owned higher electrochemical utilization, better power property, and better electrochemical stability, in contrast to the single RuO_2 phase.

2. Experimental

2.1. Synthesis of the $RuO_2 \cdot nH_2O$/MCMB Composites. Herein, the MCMB was provided by Shanshan Science and Technology Corporation (Shanghai). Its specific surface area (SSA) is *ca.* 4 $m^2 g^{-1}$ and its particle size distribution (PSD) ranged from 1 to 3 μm. The purchased MCMB was further under hydrothermal pretreatment in 6 M KOH solution at 150°C for 8 h and then washed with distilled water until the pH reached 8 [20]. The $RuO_2 \cdot nH_2O$/MCMB composites were fabricated as follows. Firstly, a certain amount of $RuCl_3 \cdot nH_2O$ was dissolved in some distilled water under stirring for 1 h to form a solution (0.018 M). Secondly, some certain amount of the pretreated MCMB was mixed into the above solution under stirring for 1 h and further ultrasonication for half an hour to form a suspension. And then the suspension was kept in a Teflon-lined autoclave with a stainless steel shell. After being kept at 180°C for 6 h in an oven [3], this autoclave was cooled to room temperature naturally. The product of the reaction was filtered, washed with distilled water and ethanol, and then dried at 80°C. The composition of the $RuO_2 \cdot nH_2O$/MCMB composites was controlled by changing the relative ratio of $RuCl_3 \cdot nH_2O$ and MCMB support in the starting mixture. The morphologies of the samples were examined by field-emission scanning electron microscope (FESEM, JEOL-6300F). The X-ray diffraction patterns of the samples were observed by XRD (Max 18 XCE Japan) using a Cu_{Ka} source.

2.2. Electrochemical Tests. The graphite electrode was first abraded with ultrafine SiC paper, rinsed in an ultrasonic bath of water for 10 minutes, and etched in a 0.5 M H_2SO_4 solution at room temperature for 40 minutes. The exposed geometric area of the graphite electrode is equal to 1 cm^2. Electrodes were prepared by mixing the active materials with acetylene black (AB) and polytetrafluoroethylene (PTFE) with the weight ratio of 10 : 1.5 : 0.5. A small amount of 0.5 M H_2SO_4 solution was then added to this composite to form a more homogeneous and coating slurry. This slurry was smeared onto the pretreated graphite substrate and then dried in a vacuum oven at 50°C overnight.

A beaker-type electrochemical cell was used for the electrochemical measurement. The cell was equipped with a working electrode, a platinum plate counter electrode, and saturated calomel electrode (SCE) reference electrode. All electrochemical measurements were done in a three-electrode system with 0.5 M H_2SO_4 solution. And all potential values in the present study are reported against the SCE. Cyclic voltammetry (CV) was evaluated by using CHI660C

electrochemical workstation. Electrochemical impedance spectroscopy (EIS) was performed with a frequency response analyzer (Solatron 1255B) interfaced with potential galvanostat (Solatron 1287) controlled by a personal computer. Chronopotentiometry (CP) curves of the electrodes were evaluated with an Arbin BT2042 battery workstation system in the certain potential ranges.

3. Results and Discussion

3.1. Characterization of the $RuO_2 \cdot nH_2O$/MCMB Composites. XRD patterns of the as-synthesized $RuO_2 \cdot nH_2O$/MCMB composites with different loadings are presented in Figure 1 as indicated. As shown in Figure 1(a), the peak intensity of the MCMB at $2\theta = 26.5°$ dramatically diminishes after loading $RuO_2 \cdot nH_2O$ NPs. Moreover, with the increase of $RuO_2 \cdot nH_2O$ NPs loadings, the peak intensity of the MCMB at $2\theta = 26.5°$ decreases more and more. Notably, the peak intensities of the MCMB from 40° to 60° also decrease greatly after loading $RuO_2 \cdot nH_2O$ NPs and keep the same decreasing trend as the peak at $2\theta = 26.5°$, as depicted in Figure 1(b). All these data support that the MCMB has been successfully coated with $RuO_2 \cdot nH_2O$ NPs after hydrothermal treatment. However, the obvious diffraction peaks of the $RuO_2 \cdot nH_2O$ phase cannot be found in Figures 1(a) and 1(b). Thus, the typical XRD pattern of $RuO_2 \cdot nH_2O$/MCMB composite with 100 wt.% $RuO_2 \cdot nH_2O$ NPs, that is, the pure $RuO_2 \cdot nH_2O$ phase, is further shown in Figure 1(b). In sharp contrast, the broad diffraction peaks with very low intensity are presented for the $RuO_2 \cdot nH_2O$ phase. And these typical diffraction peaks should result from the relative poor crystalline quality and/or nanometer-scale size of the as-prepared hydrous RuO_2 NPs. To more clearly identify the existence of RuO_2 phase in the composites, the enlarged XRD patterns of the pure $RuO_2 \cdot nH_2O$ and $RuO_2 \cdot nH_2O$/MCMB composite with 12.5 wt.% $RuO_2 \cdot nH_2O$ NPs were shown in Figure 1(c), respectively. Evidently, four obvious broad diffraction peaks contributed by the rutile RuO_2 phase (JCPDS card no. 43-1027) can be found both in the two samples, which indicates the real existence $RuO_2 \cdot nH_2O$ in the $RuO_2 \cdot nH_2O$/MCMB composites.

The FESEM images of the $RuO_2 \cdot nH_2O$/MCMB composite with the 24.8 wt.% $RuO_2 \cdot nH_2O$ NPs are shown in Figure 2. Evidently, the $RuO_2 \cdot nH_2O$/MCMB composite exhibits uniform spherical grains with the size of 1~2 μm, as shown in Figure 2(a). From the image with the higher magnification (Figure 2(b)), the nanosized $RuO_2 \cdot nH_2O$ NPs are evidently dispersed well onto the surfaces of the MCMB, the reasons for which are mainly related to the unique surface characteristics of the MCMB after the alkaline hydrothermal pretreatment. As reported before, substantial amounts of OH^- would exist upon the surfaces of the MCMB after such pretreatment [20]. The OH^- existing upon the surfaces of the MCMB not only improves the surface hydrophilic property of the MCMB but also acts as anchors for the subsequent deposition of $RuO_2 \cdot nH_2O$ NPs upon their surfaces [20]. Specifically, during stirring the suspension of the MCMB in the solution with Ru^{3+} ions, some precipitation would form onto the surfaces of the MCMB. Thus,

(a)

(b)

(c)
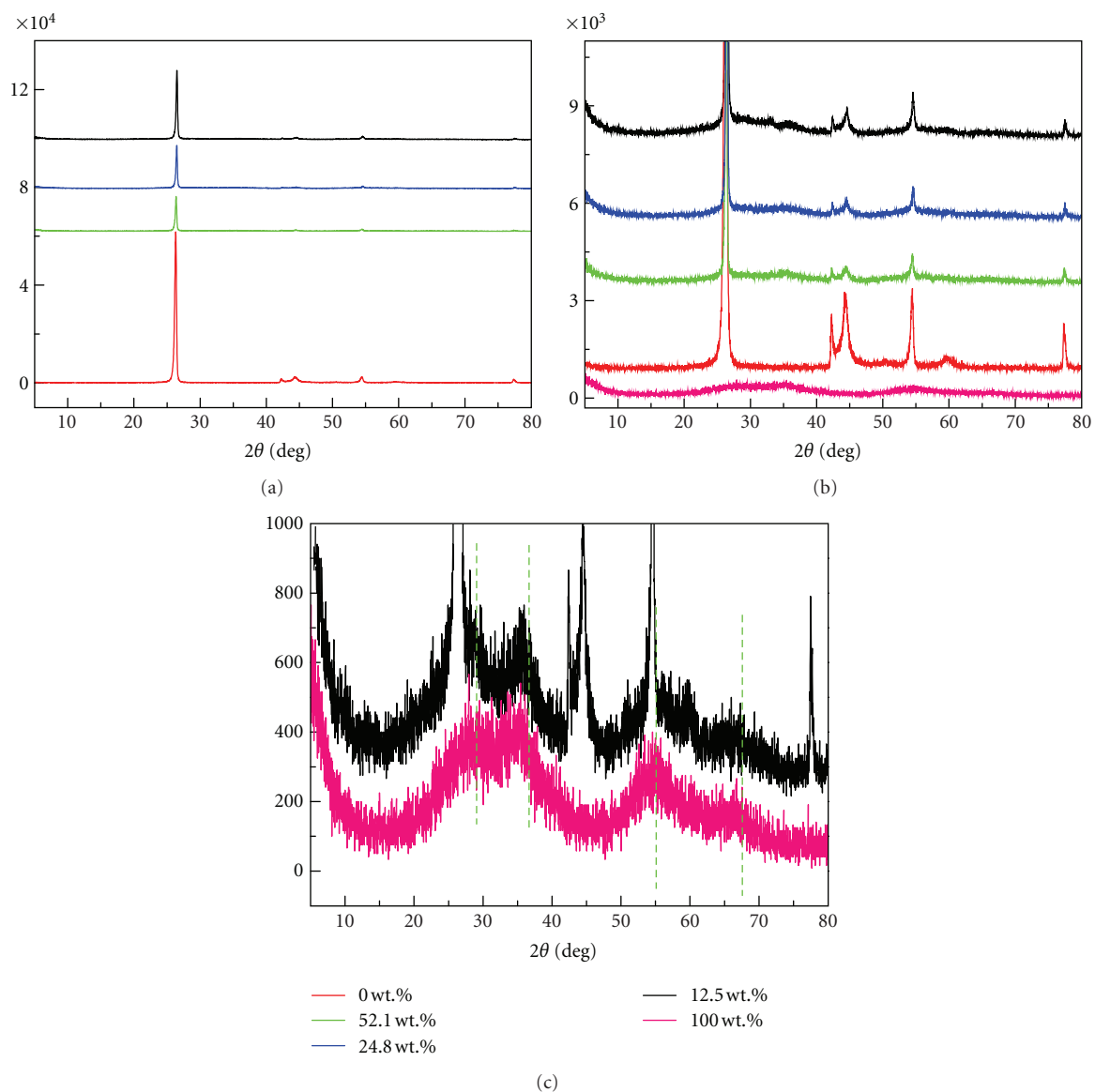
FIGURE 1: XRD patterns of $RuO_2 \cdot nH_2O$/MCMB composites with different $RuO_2 \cdot nH_2O$ loadings as indicated.

(a)

(b)
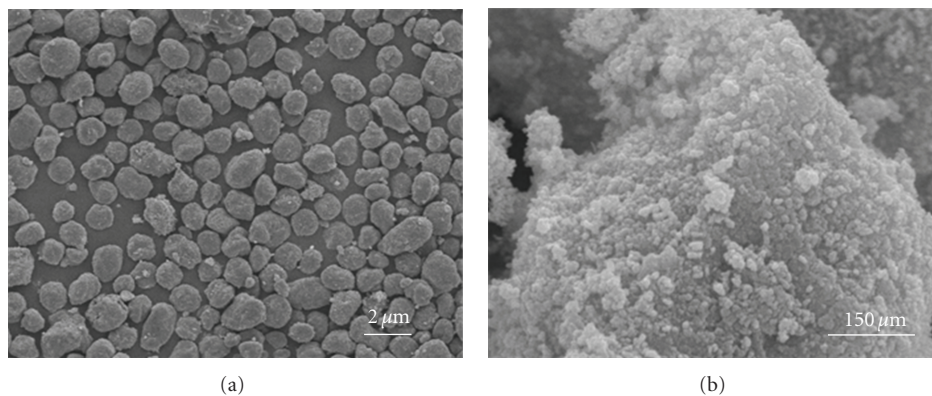
FIGURE 2: SEM images with different magnifications for the $RuO_2 \cdot nH_2O$/MCMB composite with 24.8 wt.% $RuO_2 \cdot nH_2O$ NPs.

(a)

(b)
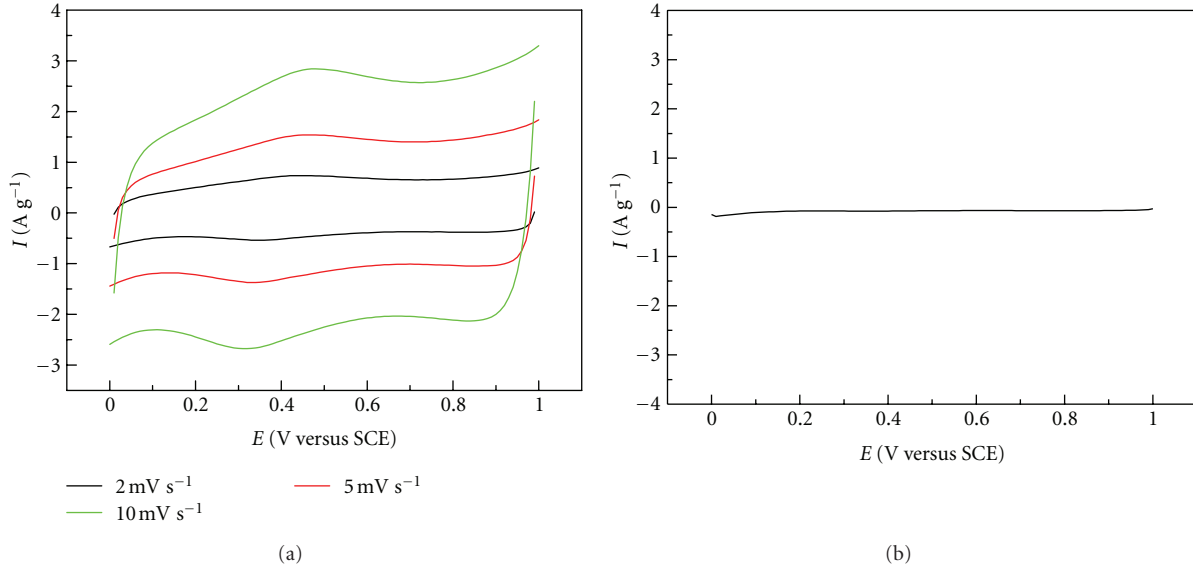
FIGURE 3: E-I curves of the $RuO_2 \cdot nH_2O$/MCMB composite electrode with 24.8 wt.% $RuO_2 \cdot nH_2O$ NPs at various scanning rates as indicated (a) and the MCMB at $10\,mV\,s^{-1}$.

with the following hydrothermal treatment at $180°C$, initial precipitation can act as nucleation centers, which results in more and more $RuO_2 \cdot nH_2O$ NPs coating onto the surfaces of the MCMB after hydrothermal treatment. Therefore, the alkaline hydrothermal treatment of MCMB plays a great role in the formation of $RuO_2 \cdot nH_2O$/MCMB composites with good dispersion of $RuO_2 \cdot nH_2O$ NPs.

3.2. Electrochemical Profiles of the $RuO_2 \cdot nH_2O$/MCMB Composites. Cyclic voltammetry was used to determine the electrochemical properties of the $RuO_2 \cdot nH_2O$/MCMB composites. Figure 3(a) shows the CV plots of the $RuO_2 \cdot nH_2O$/MCMB composite with 24.8 wt.% $RuO_2 \cdot nH_2O$ NPs in 0.5 M H_2SO_4 aqueous solution. Obviously, the CV curves of the composite all display a good rectangular shape with respect to the zero-current line and a repaid current response on voltage reversal at each end potential at various scanning rates as indicated. Also, the E-I response of the composite on the positive sweep is mirror-image symmetric to their corresponding counterpart on the negative sweep within the electrochemical window from 0.0 to 1.0 V (versus SCE), revealing a good electrochemical capacitive nature for the composite electrode in 0.5 M H_2SO_4. For comparison, the E-I response of the MCMB is also depicted in Figure 3(b). Evidently, the area under the current potential is extremely small even at $10\,mV\,s^{-1}$. It reveals that the SC of the MCMB is very little and nearly equal to zero, which should result from the low SSA of the MCMB itself. Therefore, the main phase in the composite for energy storage should be the $RuO_2 \cdot nH_2O$ NPs, rather than the MCMB phase. The typical Faradaic pseudocapacitance of the $RuO_2 \cdot nH_2O$ is demonstrated in

$$RuO_a(OH)_b + \delta H^+ + \delta e^- = RuO_{a-\delta}(OH)_{b+\delta}. \quad (1)$$
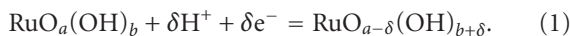
The charge-discharge study under various applied constant current densities is commonly used to examine the SC,

electrochemical reversibility, and power property of any electrode material. Thus, typical CP curves of the $RuO_2 \cdot nH_2O$/MCMB composite (24.8 wt.% $RuO_2 \cdot nH_2O$ NPs) at various current densities are shown in Figure 4(a). The E-t responses present a symmetric triangular shape, and the potential is linearly dependent on the charge-discharge time, which exhibits its good supercapacitive behavior. An important parameter, columbic efficiency (η) of the composite electrode, can be evaluated from (2) based on the CP plots depicted in Figure 4(a):

$$\eta = \frac{t_D}{t_C} \times 100\%, \quad (2)$$

where t_D and t_C are the time for galvanostatic discharging and charging, respectively. The columbic efficiencies at different current densities ranged from 0.5 to $5\,A\,g^{-1}$ all keep above 99.4%, revealing its good electrochemical reversibility.

Furthermore, the SCs of the composite electrode were calculated from the CP curves (Figure 4(a)) based on (3) and the typical data are depicted in Figure 4(b):

$$SC_{composite} = \frac{It}{\Delta V},$$
$$SC_{Ru} = \frac{SC_{composite}}{w}, \quad (3)$$

where $SC_{composite}$, SC_{Ru}, I, t, ΔV, and w are the SC ($F\,g^{-1}$) of the composite electrode, the SC ($F\,g^{-1}$) contributed by the single $RuO_2 \cdot nH_2O$ species, the charge/discharge current density ($A\,g^{-1}$), the time (s) elapsed for the discharge cycles, the potential interval (V) of the discharge, and the percentage of $RuO_2 \cdot nH_2O$ existing in the composites, respectively.

The SCs contributed by the $RuO_2 \cdot nH_2O$ species as a function of current densities are shown in Figure 4(b). Impressively, a SC_{Ru} of $1084\,F\,g^{-1}$ can be delivered at a current density of $0.5\,A\,g^{-1}$ by the composite electrode with
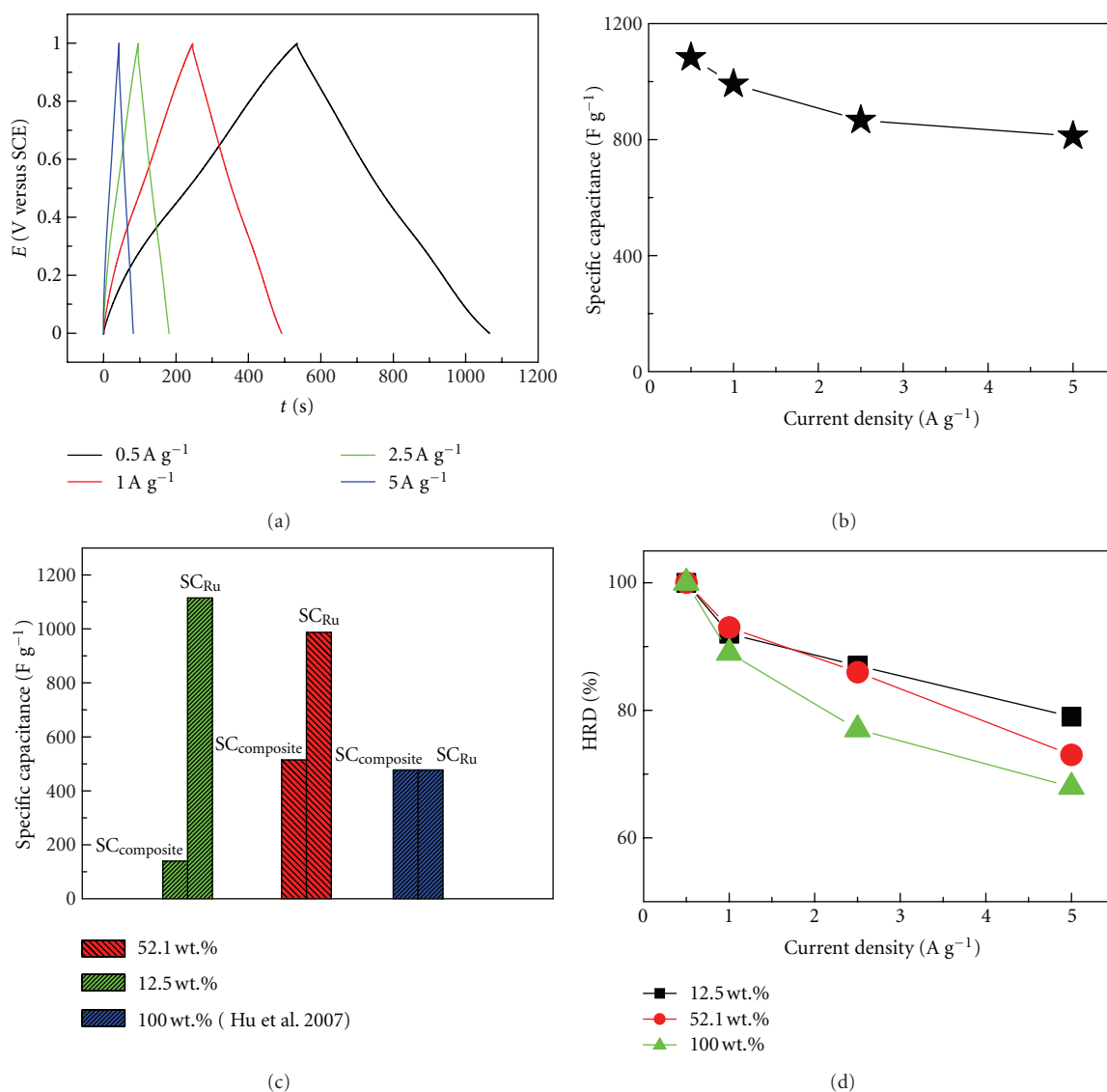
(a)

(b)

(c)

(d)

FIGURE 4: CP plots (a) and SC_{Ru} as a function of current densities (b) of the $RuO_2 \cdot nH_2O$/MCMB composite with 24.8 wt.% $RuO_2 \cdot nH_2O$; specific capacitances (c) and HRD curves (d) of the $RuO_2 \cdot nH_2O$/MCMB composites with 12.5 wt.%, 52.1 wt.% and 100 wt.% $RuO_2 \cdot nH_2O$ NPs, respectively.

24.8 wt.% $RuO_2 \cdot nH_2O$ NPs. Furthermore, the electrode not only exhibit high SCs but also maintain them well at much higher current densities. Specifically, the electrode preserves more than 74% of its SC delivered at 0.5 A/g as the current density increases to 5 A g^{-1}, that is, even 812 F g^{-1} at 5 A g^{-1}. For other composites with different $RuO_2 \cdot nH_2O$ loadings, the $SC_{composite}$ and SC_{Ru} were also estimated and collected in Figure 4(c). As reported before [3], the SC_{Ru} of the bare $RuO_2 \cdot nH_2O$, that is, the composite with 100 wt.% $RuO_2 \cdot nH_2O$ loading, is just *ca.* 477 F g^{-1}, which is much less than the SC_{Ru} of the composite electrode with 24.8 wt.% $RuO_2 \cdot nH_2O$ NPs. It indicates that the electrochemical utilization of the $RuO_2 \cdot nH_2O$ species is enhanced greatly when $RuO_2 \cdot nH_2O$ NPs are well dispersed upon the surface of the MCMB. It can be further verified by other composites with different $RuO_2 \cdot nH_2O$ loadings. As seen from Figure 4(c), the $RuO_2 \cdot$

nH_2O/MCMB composites with 12.5 wt.% $RuO_2 \cdot nH_2O$ NPs can deliver a large SC_{Ru} of 1115 F g^{-1}. In addition, a SC_{Ru} of 987 F g^{-1} still can be obtained even in the case of 52.4 wt.% $RuO_2 \cdot nH_2O$ NPs. It is worthy of noting that the $SC_{composite}$ of the composite electrode with 52.1 wt.% $RuO_2 \cdot nH_2O$ NPs is even larger than that of the bare $RuO_2 \cdot nH_2O$ NPs. Therefore, the existence of MCMB in the composites enhances the dispersion of $RuO_2 \cdot nH_2O$ NPs, which avoids the serious aggregation of $RuO_2 \cdot nH_2O$ NPs themselves and makes a great portion of ruthenium oxide NPs with large exposed surface contacted easily by the H$^+$ ions and electrons to participate in the electrochemical reaction for much efficient energy storage at high rates. Thus, a higher electrochemical utilization can be obtained for the composite electrodes.

To further determine the power performance of the electrodes, high-rate dischargeability (HRD) of the electrode was
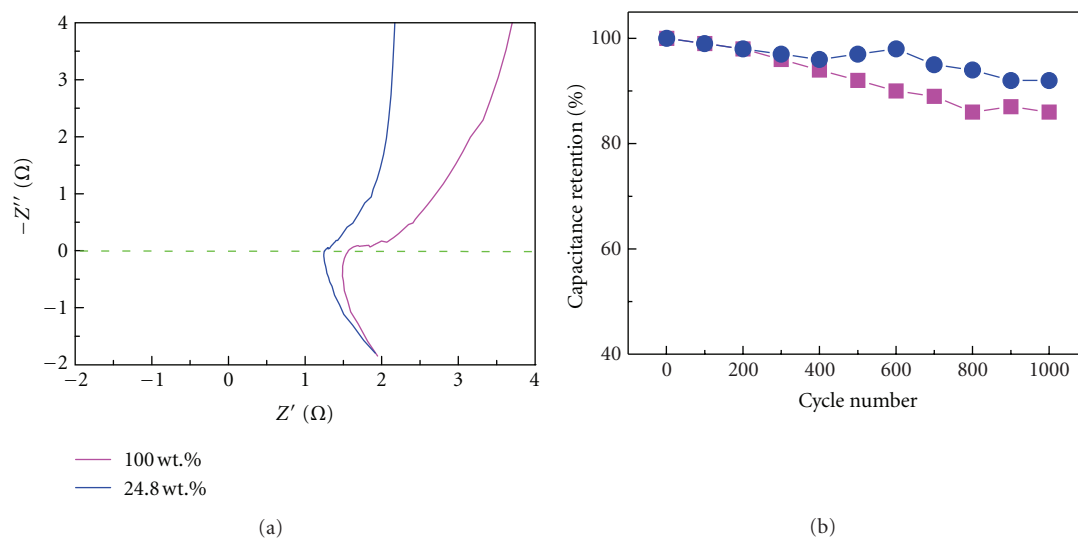
(a)

(b)

FIGURE 5: EIS plots (a) and cycling performance (b) of the $RuO_2 \cdot nH_2O$/MCMB composites with the 24.8 wt.% and 100% $RuO_2 \cdot nH_2O$ NPs, respectively.

investigated in a current density range from 0.5 to $5\,A\,g^{-1}$. Here, the HRD is defined as the ratio of SC_{Ru} at a certain current density to that at $0.5\,A\,g^{-1}$ and calculated according to

$$HRD(\%) = \frac{SC_{Ru,d}}{SC_{Ru,0.5}} \times 100, \qquad (4)$$

where $SC_{Ru,d}$ and $SC_{Ru,0.5}$ are the discharge SC_{Ru} at a certain current density and $0.5\,A\,g^{-1}$, respectively. Figure 4(d) presents the HRD properties of the composite electrodes. Clearly, the HRD of the composites with 12.5 wt.% and 52.1 wt.% $RuO_2 \cdot nH_2O$ loadings are *ca.* 73% and 79%, respectively, much higher than that of 68% for the bare $RuO_2 \cdot nH_2O$ NPs. It indicates that the composites can not only deliver large SCs but maintain them at high rates. Out of question, the existence of MCMB greatly enhances the power property of the electrodes, which is important for their practical application. The enhanced power property of the composite electrodes should be mainly related to their better electronic conductivity in contrast to that of the pure $RuO_2 \cdot nH_2O$ NPs, which can be confirmed by the following EIS data shown in Figure 5(a).

Figure 5(a) shows the complex plane plots of the $RuO_2 \cdot nH_2O$/MCMB composites with the 24.8 wt.% and 100% $RuO_2 \cdot nH_2O$ NPs, respectively. At very high frequencies, from the Nyquist plots, the intercept of the electrode with the real impedance (Z) axis reports the sum of the internal resistance of the electroactive materials, electrolyte resistance, and the contact resistance at the interface between electroactive materials and current collector [21]. Here, due to the same making technique of the three-electrode cell for test, the electrolyte resistance and the contact resistance are identical for the two electrodes. Therefore, it can be considered that the different intercepts reflect the different conductive properties of the two composite themselves. As shown from the data in Figure 5(a), the $RuO_2 \cdot nH_2O$/MCMB composite

with 24.8 wt.% $RuO_2 \cdot nH_2O$ owns much better electronic conductivity (*ca.* 1.2 ohm) than the pure $RuO_2 \cdot nH_2O$ NPs (*ca.* 1.5 ohm). Commonly, the smaller the consisting particles are, the more significant interfacial resistance between adjacent particles becomes [22]. After well dispersing $RuO_2 \cdot nH_2O$ NPs upon the surfaces of the MCMB with good electronic conductivity, the interfacial resistance can decrease to some extent.

For further understanding the electrochemical performances, the long-term cycle ability of the electrodes was also evaluated by repeating the charge/discharge test at a current density of $5\,A\,g^{-1}$ for 1000 cycles. The SC as a function of the cycle number is presented in Figure 5(b). After 1000 continuous cycle tests, the SC degradation of the $RuO_2 \cdot nH_2O$/MCMB composite with 24.8 wt.% $RuO_2 \cdot nH_2O$ is *ca.* 8%, much less than *ca.* 14% for the pure $RuO_2 \cdot nH_2O$ NPs, demonstrating that the $RuO_2 \cdot nH_2O$/MCMB composite can maintain better electrochemical stability than the single $RuO_2 \cdot nH_2O$ NPs phase.

4. Conclusions

In conclusion, an efficient hydrothermal strategy was proposed here to disperse $RuO_2 \cdot nH_2O$ NPs upon the surfaces of mesocarbon microbeads. Electrochemical capacitance of the $RuO_2 \cdot nH_2O$/MCMB composites were systematically investigated in 0.5 M H_2SO_4 aqueous solution. Electrochemical data indicated that the $RuO_2 \cdot nH_2O$/MCMB composites own higher electrochemical utilization, better power property, and better electrochemical stability than the pure $RuO_2 \cdot nH_2O$ NPs. The good dispersion of $RuO_2 \cdot nH_2O$ NPs and the enhanced electronic conductivity make the $RuO_2 \cdot nH_2O$ NPs with large exposed surface contacted easily by H^+ ions and electrons to participate in more efficient Faradaic reactions for energy storage at high rates.

Acknowledgments

References

[1] B. E. Conway, "Transition from 'supercapacitor' to 'battery' behavior in electrochemical energy storage," *Journal of the Electrochemical Society*, vol. 138, no. 6, pp. 1539–1548, 1991.

[2] G. Schlichthorl and L. M. Peter, "Impedance and microwave reflectivity measurements on n-Si in 1M LiCl/methanol I. Depletion and inversion layer formation," *Journal of the Electrochemical Society*, vol. 142, no. 8, pp. 2665–2669, 1995.

[3] C. C. Hu, K. H. Chang, and C. C. Wang, "Two-step hydrothermal synthesis of Ru-Sn oxide composites for electrochemical supercapacitors," *Electrochimica Acta*, vol. 52, no. 13, pp. 4411–4418, 2007.

[4] C. Z. Yuan, L. Chen, B. Gao, L. H. Su, and X. G. Zhang, "Synthesis and utilization of $RuO_2 \cdot xH_2O$ nanodots well dispersed on poly(sodium 4-styrene sulfonate) functionalized multiwalled carbon nanotubes for supercapacitors," *Journal of Materials Chemistry*, vol. 19, no. 2, pp. 246–252, 2009.

[5] C. C. Hu and W. C. Chen, "Effects of substrates on the capacitive performance of $RuO_x \cdot nH_2O$ and activated carbon-RuO_x electrodes for supercapacitors," *Electrochimica Acta*, vol. 19, no. 21, pp. 3469–3477, 2004.

[6] H. Kim and B. N. Popov, "Characterization of hydrous ruthenium oxide/carbon nanocomposite supercapacitors prepared by a colloidal method," *Journal of Power Sources*, vol. 104, no. 1, pp. 52–61, 2002.

[7] F. Pico, J. Ibañez, M. A. Lillo-Rodenas et al., "Understanding $RuO_2 \cdot xH_2O$/carbon nanofibre composites as supercapacitor electrodes," *Journal of Power Sources*, vol. 176, no. 1, pp. 417–425, 2008.

[8] B. J. Lee, S. R. Sivakkumar, J. M. Ko, J. H. Kim, S. M. Jo, and D. Y. Kim, "Carbon nanofibre/hydrous RuO_2 nanocomposite electrodes for supercapacitors," *Journal of Power Sources*, vol. 168, no. 2, pp. 546–552, 2007.

[9] H. Honda and Y. Yamada, "Synthesis and stability of mesocarbon microbeads separated from the mesophase pitches," *Journal of the Japan Petroleum Institute*, vol. 16, p. 392, 1973.

[10] Y. Yamada, T. Imamura, H. Kakiyama, H. Honda, S. Oi, and K. Fukuda, "Characteristics of meso-carbon microbeads separated from pitch," *Carbon*, vol. 12, no. 3, pp. 307–319, 1974.

[11] Y. G. Wang, Y. Korai, and I. Mochida, "Carbon disc of high density and strength prepared from synthetic pitch-derived mesocarbon microbeads," *Carbon*, vol. 37, no. 7, pp. 1049–1057, 1999.

[12] H. Honda, "Mesophase putch and meso-carbon microbeads," *Molecular Crystals and Liquid Crystals*, vol. 94, no. 1-2, pp. 97–108, 1983.

[13] T. Kasuh, D. A. Scott, and M. Mori, "Active carbon and processes for synthesis of same," in *Proceedings of an International Conference on Carbon, Newcastle, Extended Abstracts*, p. 146, September 1988.

[14] C. Y. Wang, H. Jiang, P. Li, and J. M. Zheng, "Structure of mesocarbon microbeads formed with original QI as seed crystal," *New Carbon Materials*, vol. 15, p. 9, 2000.

[15] R. Alcantara, F. J. Fernanfez Madrigal, P. Lavela et al., "Characterization of mesocarbon microbeads (MCMB) as active electrode material in lithium and sodium cells," *Carbon*, vol. 38, p. 1031, 2000.

[16] J. Yamaura, Y. Ozaki, A. Morita, and A. Ohta, "High voltage, rechargeable lithium batteries using newly-developed carbon for negative electrode material," *Journal of Power Sources*, vol. 43, no. 1, pp. 233–239, 1993.

[17] A. Mabuchi, K. ToKumitsu, H. fujimoto, and T. Kasuh, "Charge-Discharge Characteristics of the Mesocarbon Miocrobeads Heat-Treated at Different Temperatures," *Journal of the Electrochemical Society*, vol. 142, no. 9, pp. 1041–1046, 1995.

[18] K. Tokumitsu, H. Fujimoto, A. Mabuchi, and T. Kasuh, "High capacity carbon anode for Li-ion battery a theoretical explanation," *Carbon*, vol. 37, no. 10, pp. 1599–1605, 1999.

[19] G. Q. Zhang and X. G. Zhang, "MnO_2/MCMB electrocatalyst for all solid-state alkaline zinc-air cells," *Electrochimica Acta*, vol. 49, no. 6, pp. 873–877, 2004.

[20] C. Yuan, B. Gao, L. Su, and X. Zhang, "NiO loaded on hydrothermally treated mesocarbon microbeads (h-MCMB) and their supercapacitive behaviors," *Solid State Ionics*, vol. 178, no. 35-36, pp. 1859–1866, 2008.

[21] C. Yuan, X. Zhang, Q. Wu, and B. Gao, "Effect of temperature on the hybrid supercapacitor based on NiO and activated carbon with alkaline polymer gel electrolyte," *Solid State Ionics*, vol. 177, no. 13-14, pp. 1237–1242, 2006.

[22] C. C. Hu, W. C. Chen, and K. H. Chang, "How to achieve maximum utilization of hydrous ruthenium oxide for supercapacitors," *Journal of the Electrochemical Society*, vol. 151, no. 2, pp. A281–A290, 2004.

International Journal of
Medicinal Chemistry

Organic Chemistry
International

International Journal of
Photoenergy

International Journal of
Analytical Chemistry

Advances in
Physical Chemistry

International Journal of
Carbohydrate Chemistry

Journal of
Quantum Chemistry

The Scientific World Journal

Submit your manuscripts at
http://www.hindawi.com

Hindawi

Journal of
Analytical Methods in Chemistry

Journal of
Spectroscopy

International Journal of
Inorganic Chemistry

International Journal of
Electrochemistry

Journal of
Applied Chemistry

Bioinorganic Chemistry and Applications

Journal of
Theoretical Chemistry

Chromatography Research International

Journal of
Catalysts

Journal of
Chemistry

International Journal of
Spectroscopy